Taylor & Francis
Taylor & Francis Group

Bioacoustics
The International Journal of Animal Sound and its Recording

ISSN: 0952-4622 (Print) 2165-0586 (Online) Journal homepage: www.tandfonline.com/journals/tbio20

Form and function in the developing túngara frog (*Engystomops pustulosus*) larynx

Hans T. Bilger, Nicole M. Kime, Preston S. Wilson, Julia A. Clarke & Michael J. Ryan

To cite this article: Hans T. Bilger, Nicole M. Kime, Preston S. Wilson, Julia A. Clarke & Michael J. Ryan (21 Jan 2026): Form and function in the developing túngara frog (*Engystomops pustulosus*) larynx, Bioacoustics, DOI: 10.1080/09524622.2026.2614675

To link to this article: https://doi.org/10.1080/09524622.2026.2614675

BIOACOUSTICS
https://doi.org/10.1080/09524622.2026.2614675

Form and function in the developing túngara frog (*Engystomops pustulosus*) larynx

Hans T. Bilger[a], Nicole M. Kime[b], Preston S. Wilson[c], Julia A. Clarke[a,d] and Michael J. Ryan[a,e]

[a]Department of Integrative Biology, University of Texas at Austin, Austin, TX, USA; [b]Department of Biological Sciences, Edgewood University, Madison, WI, USA; [c]Walker Department of Mechanical Engineering, University of Texas at Austin, Austin, TX, USA; [d]Department of Geological Sciences, University of Texas at Austin, Austin, TX, USA; [e]Smithsonian Tropical Research Institute, Balboa, Republic of Panama

ABSTRACT

Male túngara frogs appear in choruses and have well-defined vocal cords at a size of 19 mm snout-vent length (SVL), but they do not begin producing advertisement calls until they reach approximately 24 mm SVL. Is this because the larynx is not fully mature until the latter point, or is it because the calls of small-bodied adults would not be attractive enough to outweigh the costs (energy, predation and parasitism) of producing them? We investigate this question by tuning bond graph models of the túngara frog larynx with parameter values across this critical body size range. Simulations were informed by a new set of diceCT-based measurements of key laryngeal morphological features from an ontogenetic series. Models produce sustained oscillations in airflow through the larynx (sound) with species-typical spectral features across the full range of the ontogenetic 'silent zone', suggesting that muteness during this period is facultative and not physically enforced. This result illuminates the morphological and behavioural consequences of an interplay of natural and sexual selection. Sexual selection and developmental constraints may lead the early development of laryngeal vibratory tissues, while natural selection (energetic costs and predation avoidance) and sexual selection (reduced call attractiveness) act to mute smaller adult frogs.

ARTICLE HISTORY
Received 12 September 2025
Accepted 2 January 2026

KEYWORDS
Vocalisation; ontogeny; morphology; sexual selection; diceCT; bond graph

Introduction

Vocal signals can be shaped by both natural and sexual selection, and sometimes the two seem to demand opposite adaptive behavioural responses. The túngara frog (*Engystomops (=Physalaemus) pustulosus*), a nocturnal amphibian from the neotropics, is one such case. Males attract females with advertisement calls, produced either alone or in choruses. Calls have two components: a *whine* and a *chuck*. Calls with only a whine are *simple*; *complex* calls append the whine with up to seven chucks. The whine is both necessary and sufficient for species recognition, and females prefer complex calls with whines and chucks of greater number and lower dominant and

CONTACT Hans T. Bilger hansbilger@utexas.edu
Supplemental data for this article can be accessed online at https://doi.org/10.1080/09524622.2026.2614675

fundamental frequencies (Ryan 1980, 1985; Rand and Ryan 1981; Wilczynski et al. 1995; Bosch et al. 2000; Akre and Ryan 2010). Advertisement vocalisations also carry costs. Vocalisation is an energetically expensive activity – the rate of oxygen consumption in calling males is 2.1 times the male's resting rate at night (Bucher et al. 1982). In addition, predators (the frog-eating bat *Trachops cirrhosus*) and parasites (the sanguivorous fly *Corethrella spp.*) are drawn to advertisement calls and prefer complex calls to simple ones (Ryan et al. 1982; Bernal et al. 2006). This leaves males with a conundrum – their acoustic displays make them both attractive to females and conspicuous to predators and parasites.

It is unknown whether the benefits of calling outweigh the costs at all points in ontogeny. Males' vocal cords become well defined at a body size of approximately 19 mm snout-vent length (SVL), but males are not observed producing calls until they reach ~24 mm SVL (Ryan 1985; Guerra et al. 2014). What accounts for the 'silent zone' between 19 and 24 mm (Figure 1(B))? It could be that (H1) despite the presence of vocal cords, the vocal production system is not yet physically developed enough to produce sound. Alternatively, perhaps (H2) males *can* call, but the acoustic features of those calls would not be attractive enough to justify the risk of producing them.

Addressing these alternative hypotheses requires new data on the morphology and biomechanics of *E. pustulosus* calls. Males produce advertisement calls using the larynx (Figure 1(A)), a multi-functional tracheal valve organ ancestral to tetrapods (Negus et al. 1957; Kingsley et al. 2018). During vocalisation in most frogs, trunk muscle contraction causes air to flow from the lungs into the posterior larynx (Martin 1971). Pressure builds in the posterior larynx, resulting in a force that acts on the vocal cords, pushing them towards the outer margins of the larynx (Gans 1973). Air then flows through the anterior larynx and into the buccal cavity

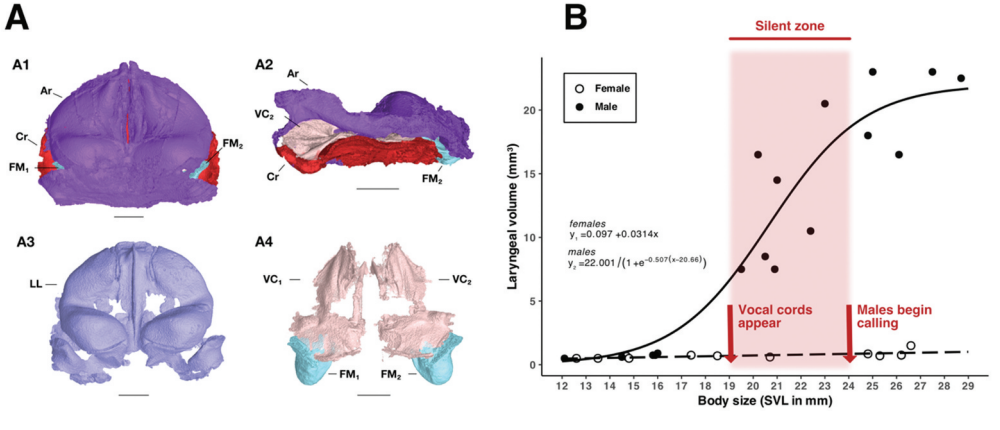

Figure 1. Anatomy and ontogeny of the male *E. pustulosus* larynx. **(A1)** Dorsal view of an adult male *E. pustulosus* larynx. **(A2)** Midsagittal view of same. **(A3)** Laryngeal lumen of same. **(A4)** Vocal cords and fibrous masses of same. Segmented from an adult male individual with an SVL of 24.7 mm. Scale bar = 1 mm. Abbreviations: Ar, arytenoid cartilage; Cr, cricoid cartilage, FM_1, fibrous mass 1; FM_2, fibrous mass 2; LL, laryngeal lumen; VC_1, vocal cord 1; VC_2, vocal cord 2. **(B)** Change in laryngeal tissue volume over the course of ontogeny in *E. pustulosus*. Males are depicted in filled circles; females are depicted in open circles. The 'silent zone' where small-bodied, non-calling males appear in choruses, occurs between ~19–24 mm SVL and is highlighted in red. Modified from Guerra et al. (2014).

through an aperture whose size is determined by the momentary displacement of the vocal cords. As air exits the larynx, the pressure inside it decreases. The vocal cords are elastic, so they begin moving back towards the laryngeal midline once their intrinsic restoring force exceeds the force exerted by residual air pressure in the posterior larynx. As they move back towards their original position, the area of the aperture between them decreases, allowing less air to escape. Air then builds up again in the posterior larynx, restarting the cycle (Kime et al. 2013). This process of passive, air-driven vocal cord oscillation is called the myoelastic-aerodynamic (MEAD) mechanism, and it is used to produce vocalisations in taxa ranging from birds to elephants to toothed whales (Herbst et al. 2012; Elemans et al. 2015; Herbst 2016; Madsen et al. 2023).

MEAD-induced vocal cord oscillations are responsible for the *whine* component of the *E. pustulosus* advertisement call, but the *chuck* appears to rely on an additional passive mechanism. *E. pustulosus* males – along with certain other anurans – have thick tissue accretions called 'fibrous masses' elastically coupled to the vocal cords (Martin 1971; Gans 1973; Drewry et al. 1982; Lagorio et al. 2020). According to the current leading hypothesis, once the fibrous masses are sufficiently excited by MEAD-induced oscillations, they collide with other structures in the larynx, generating non-linear 'impact oscillations' (Pippard 1978; Hindmarsh and Jefferies 1984; Fitch et al. 2002; Tournat et al. 2004; Bernal et al. 2009). These oscillations create subharmonics with a fundamental frequency (F_0) one-half that of the *whine* (Gridi-Papp et al. 2006; Kime et al. 2019). When the fibrous masses are surgically removed, the *chuck's* odd-order (sub-)harmonics are greatly attenuated and the call component loses its ability to make *whine*-only calls more attractive (Gridi-Papp et al. 2006; Baugh et al. 2018).

Successful call production thus seems to require, at base, (a) lungs and trunk muscles capable of generating sufficient airflow, (b) vocal cord and fibrous mass tissues with appropriate compliance, area, and mass for MEAD-induced oscillations, and (c) a larynx large enough to (i.) allow for sufficient displacement of the vocal folds and fibrous masses and (ii.) generate periodic fluctuations of air pressure in response to vocal fold displacement.

When in development does the male larynx meet these requirements? Laryngeal ontogeny in *E. pustulosus* was recently investigated by Guerra et al. (2014). Guerra and collaborators showed that male and female laryngeal tissue volume increases at a similar rate until ~16 mm SVL. At that point, male larynx tissue volume increases exponentially until 24 mm SVL, after which it resumes slow linear growth. Guerra et al. (2014) also demonstrated that juvenile *E. pustulosus* (smaller than 16 mm SVL) of both sexes lack vocal cords and fibrous masses. These data provide an ideal starting point for a bioacoustic modelling study on the ontogeny of *E. pustulosus* advertisement calls, focused on the interval during which vocal cords and fibrous masses are present but not yet deployed in sound production. We undertake that study here.

The biomechanical foundation for the present work was provided by Kime et al. (2013, 2019), who developed mathematical 'bond graph' models of anuran advertisement call production (Figure 2(A–G)). Bond graphs are a lumped-element analysis method that describe the flow of power through a dynamic physical system using equations derived from a causal model (Breedveld 2004; Karnopp et al. 2012; Borutzky 2010; Kime et al.

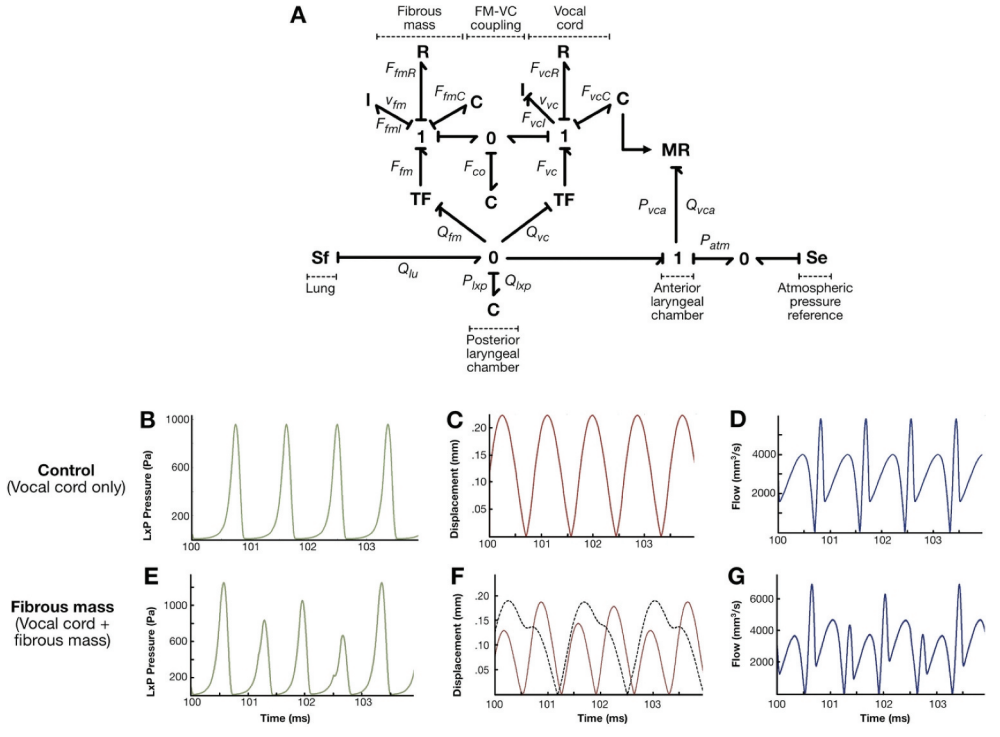

Figure 2. Bond graph model of the *E. pustulosus* vocal source. **(A)** Bond graph model used in fibrous mass and whine-chuck simulations. The model used in the whine simulation does not include the fibrous mass and the FM-VC coupling. **(B–D)** Outputs of 'control' and 'fibrous mass' models from 20-sim. Modified from Kime et al. (2019).

2013, 2019). The technique can integrate mechanical and pneumatic elements, making it particularly applicable to modelling vertebrate vocalisation. The first model created by Kime et al. (2013), referred to here as the *whine* model, successfully simulated the spectral structure of a generalised anuran *whine*-type call using parameters from prior morphological and physiological studies. This model employed a simplified representation of a generalised anuran vocal system and did not include any *E. pustulosus*-specific anatomy. A later model, referred to here as the *chuck* model, added in the fibrous mass of *E. pustulosus*. This allowed for simulation of the spectral structure of a *chuck* and the spectro-temporal structure of a *whine-chuck* call using parameters more specifically tuned to *E. pustulosus* (Kime et al. 2019). One can use these models to see how changes in suites of parameters such as vocal cord mass, fibrous mass area, or larynx volume collectively affect the dynamics of the vocal system.

Here, we study the ontogeny of advertisement call production in *E. pustulosus* by pairing Kime et al.'s (2013, 2019) bond graph models with new morphological data derived in part from Guerra et al.'s (2014) ontogenetic dataset. First, excised larynx specimens in the Guerra et al. (2014) study were re-analysed using diffusible iodine-based contrast-enhanced CT (diceCT) imaging. This imaging approach allowed for additional measurements to be taken and offered a more detailed assessment of laryngeal morphology, especially across later ontogenetic

stages. The dataset was then expanded with whole-body diceCT scans of *E. pustulosus* juveniles and adult males, which further increased the range of possible morphological measurements. Once laryngeal parameters were measured and estimated for each specimen, their values were used to 'tune' bond graph models developed by Kime et al. (2013, 2019). Model simulation outputs allowed for the inference of (a) when in ontogeny the larynx can produce sustained oscillations of the vocal cords and airflow through the larynx, (b) the relationship between body size and *whine* and *chuck* fundamental/dominant frequencies, and (c) the emergence point and character of nonlinear dynamics in the larynx. These features, in turn, supply a line of evidence to test alternative hypotheses for the existence of the 'silent zone' in male *E. pustulosus* development.

Materials and methods

In order to measure and estimate key vocal parameters across ontogeny, 30 excised male and female *E. pustulosus* larynges from the original dataset compiled for Guerra et al. (2014) were imaged using diceCT (Gignac et al. 2016). The sample included 13 females ranging in body length from 12.6 to 28.0 mm SVL and 17 males ranging from 12.1 to 28.7 mm SVL. Staining and scanning were conducted by Dr. Jessica Maisano and Dr. Matthew Colbert at The High-Resolution X-ray Computed Tomography Facility at The University of Texas at Austin (UTCT). Of the 30 excised larynges, 28 were then segmented and measured using VGSTUDIO (ver. 3.5; www.volumegraphics.com).

Some morphological measurements (e.g. vocal cord area) were not recoverable from the excised larynx specimens due to tissue deformation, so the sample from Guerra et al. (2014) was supplemented with six additional full-body diceCT scans – three of adult males, and three of juveniles of unknown sex. Full-body adult and excised larynx specimens are reposited in the Texas Natural History Collections at the University of Texas at Austin. Full-body juvenile specimens were loaned by Dr. Marcos Gridi-Papp of the University of the Pacific. Specimen numbers, staining details, and diceCT scanning parameters can be found in Table S1.

Measuring and estimating key vocal parameters across ontogeny

Morphological and physiological parameters listed in Table 1 were sourced and estimated from newly collected diceCT measurements, Guerra et al. (2014), and other prior literature. diceCT allows for micron-scale resolution of soft tissues, but tissues are also known to shrink over the course of staining (Gignac et al. 2016). For each parameter, an attempt was made to choose the most suitable measurement source and to correct for potential shrinkage effects. Certain parameters – namely (1) the compliance of the tissue composing the vocal cords, fibrous masses, and their coupling, and (2) the damping ratio of vocal cord and fibrous mass tissue – could not be measured from diceCT data and have not been reported elsewhere in the literature. Since there appears to be no evidence suggesting that these parameter values change over the course of ontogeny, they were held constant in all simulations at the values published in the original bond graph models (Kime et al. 2013, 2019). Airflow rate from one lung was a particularly important

Table 1. Parameters used in bond graphs. Methods used for calculating anatomical and physiological parameters can be found in Supplementary Materials.

Parameter	Calculated in present study?	Value
Mass of fibrous mass	Yes	Variable
Mass of vocal fold	Yes	Variable
Effective area of vocal fold	Yes	Variable
Effective area of fibrous mass	Yes	Variable
Fibrous mass displacement at lateral boundary	Yes	Variable
Larynx radius	Yes	Variable
Posterior laryngeal chamber volume (half)	Yes	Variable
Radius of fixed aperture (assumed to be equal to vocal cord length)	Yes	Variable
Flow rate during chuck (one lung)	Yes	Variable
Whine final flow rate (one lung)	Yes	Variable
Whine initial flow rate (one lung)	Yes	Variable
Vocal cord damping ratio	No	0.1
Fibrous mass damping ratio	No	0.1
Vocal cord compliance	No	0.2 m/N
Vocal cord compliance at median of larynx	No	1×10^{-5} m/N
Compliance of vocal cord-fibrous mass coupling	No	0.6 m/N
Density of air	No (physical constant)	1.21 kg/m^3
Speed of sound in air	No (physical constant)	343 m/s
Discharge coefficient through orifice	No (physical constant)	0.62

parameter for this study. It was estimated across the studied range of body sizes through linear extrapolation from an average flow rate measured physiologically from an adult frog in a prior study (Dudley and Rand 1991). Initial and final flow rates for the whine were calculated by multiplying the allometrically corrected average flow rate by a scaling factor used in Kime et al.'s (2019) prior call modelling study (Fig. S4). A full description of parameter measurement methods can be found in Supplementary Materials.

Tuning bond graph models from Kime et al. (2013, 2019)

Once larynx and airflow parameters had been measured and estimated, they were used to tune the anuran vocalisation models (Figure 2(A)) created by Kime et al. (2013, 2019). All models are 'half-larynx' models, meaning that they only include one vocal cord, one fibrous mass, and air from one lung. Kime et al.'s (2013) model, here referred to as the '*whine*' model, includes the vocal cords only, without the fibrous mass. (Note that the fibrous mass, while apparently not necessary for *whine* production, still plays a minor role in shaping aspects of the call's spectral structure (Gridi-Papp et al. 2006; Kime et al. 2019).) Kime et al.'s (2019, Figure 2) model, here referred to as the '*chuck*' model, includes a fibrous mass attached to the vocal cord with an elastic coupling. Models were built and simulations run in 20-sim (Version 4.8, Controllab Products, B.V.), a commercial software program created for the modelling and simulation of mechatronic systems. *In vivo*, airflow rate varies dynamically over the course of a call, but in the present study, along with the prior studies by Kime et al. (2013, 2019), a single airflow rate was used for both *whine* and *chuck* simulations due to uncertainty around the precise dynamics of this process. Within the *whine-chuck* simulations, airflow and vocal cord compliance were dynamically varied to attempt to produce the *complex* advertisement calls of *E. pustulosus*.

For each specimen in the sample, *whine* and *chuck* simulations were run with the measured and estimated parameters for that individual. Model outputs included pressure

within the posterior laryngeal chamber, displacement of the vocal folds, and airflow rate through the vocal fold aperture. A *whine* simulation was considered successful if it produced sustained oscillations of vocal cord displacement and air pressure in the posterior larynx (*sensu* Kime et al. 2013, 2019). Fast Fourier transform (FFT) analysis was then conducted to measure the fundamental frequency of the oscillations.

Chuck simulations had two criteria of success. The first was sustained oscillations of the vocal cord, fibrous mass, and pressure in the posterior larynx. The second was a nonlinear bifurcation caused by collision of the fibrous mass with the laryngeal midline. FFT analysis was conducted to measure fundamental and dominant frequencies of *chuck* model oscillations.

Following *whine* and *chuck* model simulations, a *whine-chuck* simulation was run using the same parameters. The output of this model was resampled at 96 kHz and converted to a spectrogram to assess its acoustic similarity to a species-typical *whine-chuck* call. Spectrograms were produced in R v4.5.2 (R Core Team, 2025), and scripts used for their production are available in Open Science Framework (see Data Availability Statement). Since the *whine-chuck* model includes significant assumptions about dynamic changes in airflow rate and vocal cord compliance – two parameters that were not measured in the present study – it was assigned a secondary role in our analysis. The following analyses primarily focus on the better constrained *whine* and *chuck* models.

Assessment of airflow thresholds

If *whine* or *chuck* models produced sustained oscillations, a further analysis was conducted to determine the minimum airflow rate sufficient to generate the oscillations. The distance between this threshold value and the estimated average airflow gives a sense of the operational range of the larynx at a given point in ontogeny. To determine minimum airflow rate, airflow rate was decreased from its predicted average value in increments smaller than or equal to 0.05×10^{-6} m^3/s until (a) the *whine* model stopped producing sustained vocal cord oscillations and (b) the *chuck* model stopped producing fibrous mass impact oscillations. For models that did not produce sustained oscillations at predicted average flow rates, fundamental frequency was measured at the minimum flow rate necessary to produce sustained oscillations.

Statistical analyses

To quantify ontogenetic trends in laryngeal morphology and model outputs (Figures 3–5), we used ordinary least squares linear regressions with snout – vent length (SVL) as the predictor and each measured or estimated morphological or model output value as the response variable. Analyses were conducted in R v4.5.2 (R Core Team, 2025) using the base function 'lm'. Following Davis and Kay (2023), we evaluated linear-model assumptions by inspecting residual vs. fitted plots (linearity and homoscedasticity) and quantile – quantile plots of residuals (normality), and by performing Shapiro–Wilk tests of residual normality and Breusch – Pagan tests of homogeneity of variance. In all cases used for inference, there was no strong evidence of serious violations of these assumptions. Regression lines shown in (Figures 3–5) are based on these models; reported p-values refer to the corresponding slope terms. For strictly positive, right-skewed variables (i.e. Figures 4(C) and 5(D)) we

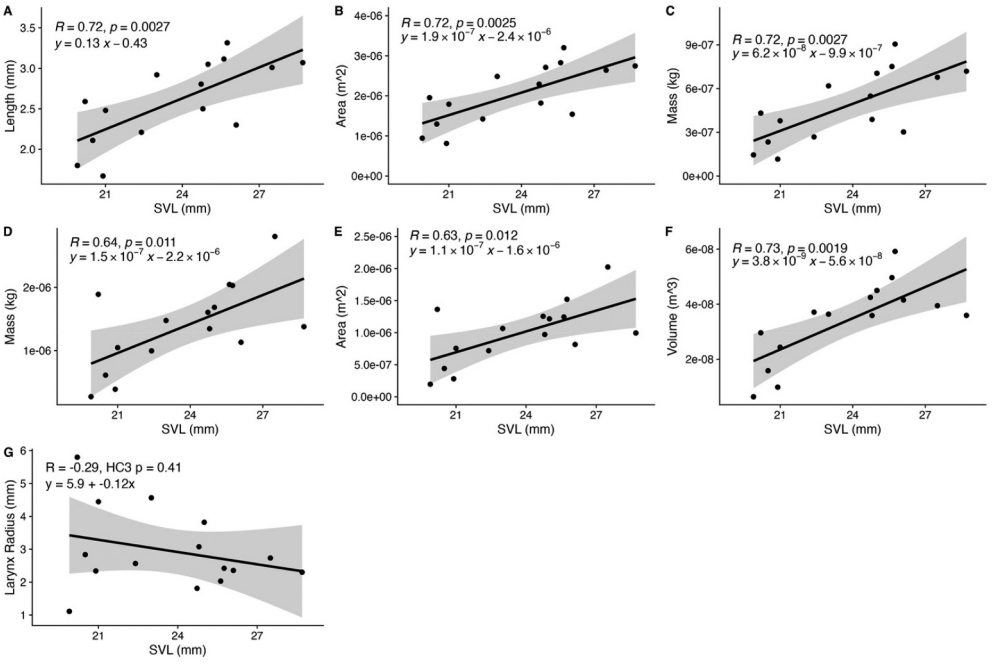

Figure 3. Ontogeny of laryngeal elements in male *E. pustulosus* between 19–29 mm SVL. **(A)** Vocal cord length vs. body length. **(B)** Vocal cord area vs. body length. **(C)** Vocal cord mass vs. body length. **(D)** Fibrous mass mass vs. body length. **(E)** Fibrous mass area vs. body length. **(F)** Posterior larynx volume vs. body length. **(G)** Mediolateral larynx radius vs. body length.

applied log10 transformations prior to analysis to improve linearity and stabilise variances. One model (Figure 3(G)) showed evidence of heteroscedasticity that was not resolved by transformation (Breusch – Pagan test, $p < 0.05$). Here, we report heteroscedasticity-consistent (HC3) standard errors for regression coefficients.

Results

Whine model

For *whine* models tuned with parameters from male *E. pustulosus* 19 mm SVL or larger (Figure 3; Table 2), 9 out of 15 simulations produced sustained oscillations using average flow rates predicted by linear extrapolation from the flow rate and body size of an adult frog measured in a prior study (Dudley and Rand 1991, see Supplementary Materials). The remaining six simulations produced sustained oscillations using flow rates within the relative range of flow rate increase used by Kime et al. (2019) in the *whine-chuck* model (i.e. ±66%). The predicted fundamental frequency for a male with a body length of 19 mm SVL was 1398 Hz; for a male with an SVL of 30 mm (the 'silent zone', to reiterate, usually ends around 24 mm SVL), the predicted fundamental frequency was 419 Hz (Figure 4(A)). In nature, the *whine* call typically sweeps from approximately 900–430 Hz (Ryan 1985). The minimum airflow rate required to produce the whine increased with body length (Figure 5(A)).

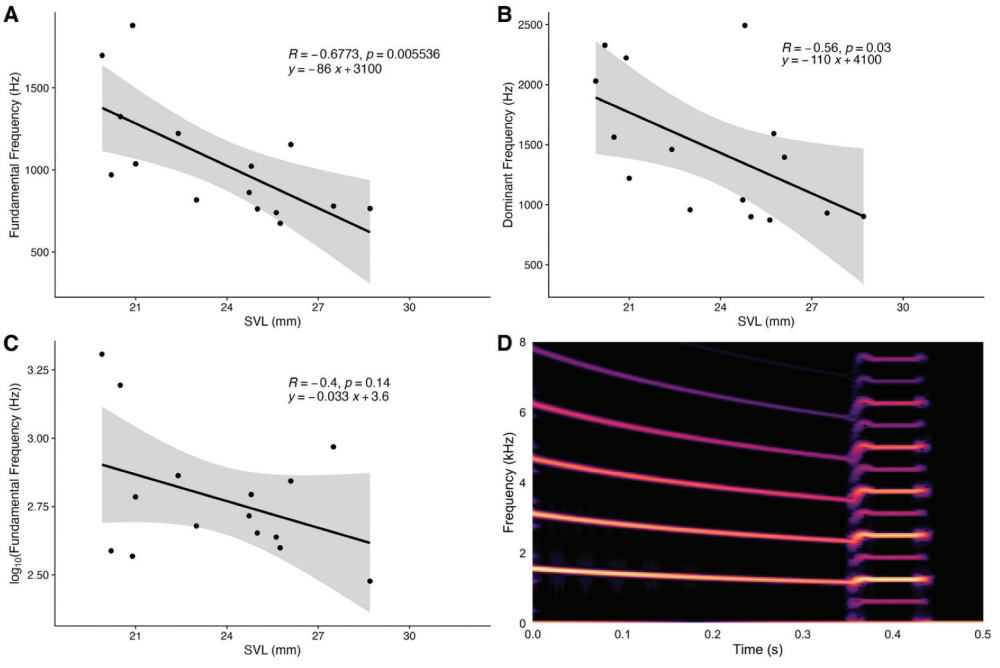

Figure 4. Bond graph model outputs. **(A)** Fundamental frequencies of sustained vocal cord oscillations produced by *whine* model for adult males larger than 19 mm SVL. **(B)** Dominant frequencies of sustained vocal cord and fibrous mass oscillations produced by *chuck* model for adult males larger than 19 mm SVL. **(C)** Fundamental frequencies of sustained vocal cord and fibrous mass oscillations produced by *chuck* model for adult males larger than 19 mm SVL. **(D)** A simulated *whine-chuck* call produced by the *whine-chuck* model using parameters from specimen TNHC 85849 (SVL = 24.8 mm). All *whine* and *chuck* models produced sustained oscillations when given measured and estimated parameters for male *E. pustulosus* specimens larger than 19 mm, but not all *whine-chuck* models produced species typical *whine-chuck* calls.

Chuck model

All *chuck* models tuned with parameters from male *E. pustulosus* 19 mm SVL or larger (Figure 3; Table 2) produced sustained oscillations and fibrous mass impact oscillations with predicted average flow rates. For an individual of 19 mm SVL, the *chuck* model predicted a fundamental frequency of 1055 Hz and a dominant frequency of 1993 Hz. For an individual of 30 mm SVL, it predicted a fundamental frequency of 235 Hz and a dominant frequency of 757 Hz (Figure 4(B)). In nature, *chucks* have a fundamental frequency one-half that of the whine (i.e. 215–450 Hz) and a dominant frequency of ~2550 Hz (Ryan 1985). (Comparison of model-generated dominant frequencies with those of living *E. pustulosus* males is deceptive, however. The dominant frequency of a vocalisation can be greatly affected by the transfer function of the upper vocal tract, and the models used here do not include an upper vocal tract.) The minimum airflow rate required to produce sustained oscillations increased with body size (Figure 5(B)), but it was significantly lower than for the *whine* models – most specimens required a 2–4x higher airflow rate to sustain oscillations in the *whine* model than in the *chuck* model

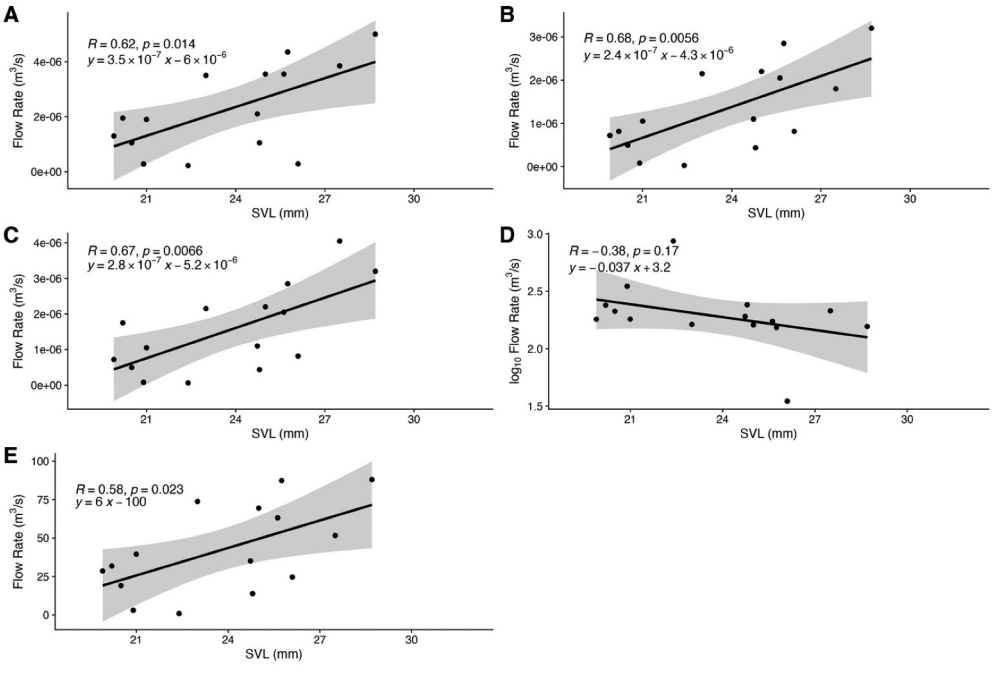

Figure 5. Flow rates. **(A)** The minimum flow rate from one lung necessary to induce sustained vocal cord oscillations in the *whine* model for each adult male specimen larger than 19 mm SVL. **(B)** The minimum flow rate from one lung necessary to induce sustained oscillations of the vocal cords and fibrous mass in the *chuck* model for each adult male specimen larger than 19 mm SVL. **(C)** The minimum flow rate from one lung necessary to induce impact oscillations in the fibrous mass in the *chuck* model for each adult male specimen larger than 19 mm SVL. **(D)** The percentage difference in minimum flow rate necessary to produce sustained oscillations in the whine and chuck models. The whine model took an average of 234% more flow to produce sustained oscillations than the chuck model. **(E)** Percentage of estimated average flow rate required to produce sustained oscillations in the vocal cord and fibrous mass in the *chuck* model.

(Figure 5(C)). The magnitude of the minimum flow rate relative to the predicted average flow rate also increased with body size in the *chuck* model (Figure 5(E)).

Whine-chuck model

Only two simulations produced species-typical *whine-chuck* calls – those with parameters from specimens TNHC 85849 (Figure 4(D)) and TNHC 85850. Other models either produced no sustained oscillations or (more commonly) some abnormal mixture of sustained oscillations, subharmonics and other non-linear phenomena, and chaotic noise. Exploratory analyses suggested that the value of the compliance of the vocal cord-fibrous mass coupling has a large influence on whether or not the fibrous mass produces the impact oscillations hypothesised to be crucial to the *chuck* spectral structure.

Table 2. Parameters used to tune whine and chuck bond graph models for male specimens with well-defined vocal cords. M_{fm}, mass of fibrous mass (single); M_{vc}, mass of vocal cord (single); X_{vc-lb}, displacement of vocal cord at lateral boundary (equal to mediolateral radius of larynx); L_{vc} length of vocal cord (single); C_{lxp}, compliance of air in posterior larynx; A_{fm}, effective area of fibrous mass (single); A_{vc}, effective area of vocal cord (single).

Specimen	Sex	SVL (mm)	M_{fm} (kg)	M_{vc} (kg)	X_{vc-lb} (m)	C_{lxp} (m^3/Pa)	L_{vc} (mm)	Flow rate from one lung (m^3/s)	A_{fm} ($1/m^2$)	A_{vc} ($1/m^2$)
85843	M	19.9	2.71E-07	1.45E-07	1.11E-03	4.47E-14	1.8	2.52E-06	5.11E + 06	1.06E + 06
85846	M	20.2	1.89E-06	4.32E-07	5.80E-03	2.08E-13	2.59	2.56E-06	7.34E + 05	5.12E + 05
85841	M	20.5	6.12E-07	2.33E-07	2.84E-03	1.11E-13	2.11	2.60E-06	2.27E + 06	7.71E + 05
85842	M	20.9	3.89E-07	1.16E-07	2.34E-03	6.92E-14	1.67	2.65E-06	3.57E + 06	1.23E + 06
85844	M	21	1.05E-06	3.79E-07	4.45E-03	1.71E-13	2.48	2.66E-06	1.32E + 06	5.58E + 05
85848	M	22.4	9.96E-07	2.68E-07	2.57E-03	2.61E-13	2.21	2.84E-06	1.39E + 06	7.03E + 05
85858	M	23	1.48E-06	6.19E-07	4.56E-03	2.55E-13	2.92	2.91E-06	9.39E + 05	4.03E + 05
40573	M	24.73	1.61E-06	5.48E-07	1.81E-03	2.98E-13	2.81	3.13E-06	7.97E + 05	4.36E + 05
85849	M	24.8	1.35E-06	3.88E-07	3.08E-03	2.52E-13	2.50	3.14E-06	1.03E + 06	5.49E + 05
85855	M	25	1.69E-06	7.05E-07	3.82E-03	3.16E-13	3.05	3.17E-06	8.23E + 05	3.69E + 05
40580	M	25.62	2.05E-06	7.51E-07	2.03E-03	3.49E-13	3.12	3.25E-06	8.03E + 05	3.54E + 05
31539	M	25.75	2.03E-06	9.05E-07	2.42E-03	4.16E-13	3.32	3.26E-06	6.58E + 05	3.12E + 05
85850	M	26.1	1.13E-06	3.02E-07	2.36E-03	2.92E-13	2.30	3.31E-06	1.23E + 06	6.49E + 05
85854	M	27.5	2.81E-06	6.78E-07	2.73E-03	2.77E-13	3.01	3.48E-06	4.94E + 05	3.79E + 05
85832	M	28.7	1.38E-06	7.19E-07	2.30E-03	2.52E-13	3.07	3.64E-06	1.01E + 06	3.64E + 05

Discussion

Bond graph models of *E. pustulosus* tuned with parameters realistic for males approximately 19 mm SVL and larger produce sustained oscillations of pressure/vocal cord displacement and are able to generate key spectral features of *E. pustulosus* advertisement calls (i.e. subharmonics/non-linear behaviour). These results suggest that male frogs are capable of vocalising during the 'silent zone' in their development (19–24 mm SVL) and that their apparent facultative muteness could be the result of an evolutionary trade-off between the benefits of call production in terms of mate attraction and its costs in terms of energy and predation risk.

Facultative muteness in small males could occur because they are incapable of producing identifiable or attractive signals. The present study's simulation outputs suggest that it is unlikely that small males could produce calls that are recognised as conspecific. Females require a low-frequency portion of the *whine* in the range of 500–640 Hz in order to recognise the caller as a conspecific (Wilczynski et al. 1995; Page and Bernal 2006), markedly lower than the fundamental frequency of 1398 Hz predicted by the *whine* simulation for an individual of 19 mm SVL. Similarly, small males in a chorus of larger males may be disfavoured by females. Females are known to prefer whines with lower dominant frequencies and chucks with lower fundamental and dominant frequencies (Ryan 1980, 1985; Rand and Ryan 1981; Wilczynski et al. 1995; Bosch et al. 2000).

Female conspecific recognition abilities and call preferences are partially determined by the tuning of the species' two auditory organs: The amphibian papilla, responsible for perceiving low-frequency sounds, is most sensitive around 700 Hz, and the basilar papilla, responsible for perceiving higher-frequency sounds, is most sensitive around 2130 Hz (Ryan et al. 1990). These behavioural and physiological facts suggest that the *whines* of small-bodied adult males perhaps would not reach low enough frequencies to allow for species recognition or be attractive enough to be chosen by females in choruses where larger males are also present.

A chief advantage of the bond graph models used in the present study is that they allow for the investigation of a suite of anatomical and physiological changes over development (Kime et al. 2013). While it is intuitive that a larger larynx would produce lower-pitched sounds, this outcome is not inevitable. In the present study, parameters such as vocal cord mass, fibrous mass area, and larynx volume are all correlated positively with body size, and body size is correlated negatively with the fundamental frequencies of *whine* and *chuck* simulations. But since these characteristics all follow their own distinct ontogenetic trajectories, it is unclear whether, at any one time point, the combined characteristics of vocal system morphology could support vocal production or create a specific spectral structure.

The importance of considering the whole vocal system is evident in the development of the bond graph model itself over successive studies. *In vivo*, an adult *E. pustulosus* frog with a body size of ~30 mm SVL produces a *whine* whose F_0 sweeps from ~900–430 Hz; *chucks* have an F_0 of 215–415 Hz (Ryan 1985). Kime et al.'s (2019) *whine* model produced a F_0 of 1145 Hz for a frog of similar size; the *chuck* model produced an F_0 1435 Hz. With the new parameter values of the present study, however, the simulation outputs more closely mirrored *in vivo* values: *whine* simulations for 30 mm males produced an F_0 of 419 Hz; chuck simulations produced an F_0 of 235 Hz. These results underscore how a deterministic nonlinear

system such as the vocal mechanism can be subject to the 'butterfly effect', where specific initial parameter values can lead to starkly diverging simulation outputs, even in models with the same basic elements (Fitch et al. 2002; Lorenz 1963). Continued modelling, physiological, and biomechanical studies are needed to increase our knowledge of the *E. pustulosus* vocal system, such as the effects of dynamic changes in vocal tissue compliance and airflow on the spectrotemporal structure of advertisement calls.

Evidence from bond graph simulations suggests that the cost of signal production outweighs the potential benefits of mate attraction during the 'silent period' of *E. pustulosus* ontogeny. Phonotaxis experiments could test whether or not females recognise or prefer synthesised calls from different points in ontogeny. If females do not recognise the synthesised calls of small-bodied adult males or prefer the calls of larger-bodied ones, it would be consistent with the findings reported here.

Acknowledgements

The authors thank Dr. Monica Guerra for collecting and preparing the original ontogenetic series of laryngeal samples, Dr. Jessica Maisano for diceCT scanning of specimens, Dr. Travis Laduc and Dr. Marcos Gridi-Papp for facilitating specimen loans, and Luke Larter for editorial input on the manuscript.

Author contributions

Conceptualization: MJR, JAC, NMK, HTB, PSW; Methodology: HTB, NMK, PSW, MJR, JAC; Data curation: HTB; Formal analysis: HTB, NMK; Investigation: HTB, NMK, JAC, MJR; Visualization: HTB; Funding acquisition: HTB; Project administration: HTB; Writing – original draft: HTB; Writing – review & editing: HTB, MJR, JAC, NMK, PSW; Supervision: MJR, JAC, PSW.

Disclosure statement

No potential conflict of interest was reported by the author(s).

Funding

This work was supported by National Science Foundation Graduate Research Fellowship Program [Fellow ID 2018262669, awarded to HTB]; German Academic Exchange Service (DAAD; Research Grant for Doctoral Candidates and Young Academics and Scientists) [Funding Program #57381410, awarded to HTB]; Howard Hughes Medical Institute [#GT10473, awarded to JAC] and the University of Texas at Austin (EEB Enhanced Support Fellowship and Ecology and Evolutionary Biology Research Grants awarded to HTB).

Data availability

Upon publication, all data will be available in the manuscript, the supplementary materials, and on Open Science Framework (https://osf.io/nhxy7/overview?view_only=7ddff5a63d9e4327a1b127df11fae1db). Reconstructed CT scan data are available on MorphoSource (https://www.morphosource.org/projects/000800763?locale=en) and upon request.

Generative artificial intelligence (AI)

ChatGPT 5 (Open AI, Sep 10 version) and Chat GPT 5.2 (Open AI, Dec 17 version) were used to plot the data and best-fit lines in Figure 1B, and to assist with testing of linear model assumptions in Figures 3, 4, and 5. All code was rigorously checked for accuracy and revised where necessary; best fit equations were also independently verified using Wolfram|Alpha (Wolfram, 11 September version) to ensure accuracy.

References

Akre KL, Ryan MJ. 2010. Proximity-dependent response to variably complex mating signals in túngara frogs (*Physalaemus pustulosus*). Ethology. 116(12):1138–1145. https://doi.org/10.1111/j.1439-0310.2010.01825.x

Baugh AT, Gridi-Papp M, Ryan MJ. 2018. A laryngeal fibrous mass impacts the acoustics and attractiveness of a multicomponent call in túngara frogs (*Physalaemus pustulosus*). Bioacoustics. 27(3):231–243. https://doi.org/10.1080/09524622.2017.1317288

Bernal XE, Page RA, Ryan MJ, Argo TF IV, Wilson PS. 2009. Acoustic radiation patterns of mating calls of the túngara frog (*Physalaemus pustulosus*): implications for multiple receivers. J Acoustical Soc Am. 126(5):2757–2767. https://doi.org/10.1121/1.3212929

Bernal XE, Rand AS, Ryan MJ. 2006. Acoustic preferences and localization performance of blood-sucking flies (*Corethrella Coquillett*) to túngara frog calls. Behav Ecol. 17(5):709–715. https://doi.org/10.1093/beheco/arl003

Borutzky W. 2010. Bond graph based physical systems modelling. In: Bond graph methodology: development and analysis of multidisciplinary dynamic system models. Springer; pp 17–88. https://doi.org/10.1007/978-1-84882-882-7_2

Bosch J, Rand AS, Ryan MJ. 2000. Signal variation and call preferences for whine frequency in the túngara frog, *Physalaemus pustulosus*. Behav Ecol Sociobiol. 49(1):62–66. https://doi.org/10.1007/s002650000280

Breedveld PC. 2004. Port-based modeling of mechatronic systems. Math Comput Simul. 66(2–3):99–128. https://doi.org/10.1016/j.matcom.2003.11.002

Bucher TL, Ryan MJ, Bartholomew GA. 1982. Oxygen consumption during resting, calling, and nest building in the frog *Physalaemus pustulosus*. Physiol Zool. 55(1):10–22. https://doi.org/10.1086/physzool.55.1.30158439

Davis AJ, Kay S. 2023. Writing statistical methods for ecologists. Ecosphere. 14(5):e4539.

Drewry GE, Heyer WR, Rand AS. 1982. A functional analysis of the complex call of the frog *Physalaemus pustulosus*. Copeia. 1982(3):636–645. https://doi.org/10.2307/1444664

Dudley R, Rand AS. 1991. Sound production and vocal sac inflation in the túngara frog, *Physalaemus pustulosus* (Leptodactylidae). Copeia. 1991(2):460–470. https://doi.org/10.2307/1446594

Elemans CP et al. 2015. Universal mechanisms of sound production and control in birds and mammals. Nat Commun. 6(1):8978. https://doi.org/10.1038/ncomms9978

Fitch WT, Neubauer J, Herzel H. 2002. Calls out of chaos: the adaptive significance of nonlinear phenomena in mammalian vocal production. Anim Behav. 63(3):407–418. https://doi.org/10.1006/anbe.2001.1912

Gans C. 1973. Sound production in the salientia: mechanism and evolution of the emitter. Am Zool. 13(4):1179–1194. https://doi.org/10.1093/icb/13.4.1179

Gignac PM et al. 2016. Diffusible iodine-based contrast-enhanced computed tomography (diceCT): an emerging tool for rapid, high-resolution, 3-D imaging of metazoan soft tissues. J Anat. 228(6):889–909. https://doi.org/10.1111/joa.12449

Gridi-Papp M, Rand AS, Ryan MJ. 2006. Complex call production in the túngara frog. Nature. 441(7089):38–38. https://doi.org/10.1038/441038a

Guerra MA, Ryan MJ, Cannatella DC. 2014. Ontogeny of sexual dimorphism in the larynx of the túngara frog, *Physalaemus pustulosus*. Copeia. 2014(1):123–129. https://doi.org/10.1643/CG-13-051
Herbst CT. 2016. Biophysics of vocal production in mammals. In: Suthers RA, Fitch WT, Fay RR, & Popper AN, editors. Vertebrate sound production and acoustic communication. Springer. p. 159–189. https://doi.org/10.1007/978-3-319-27721-9_6
Herbst CT et al. 2012. How low can you go? Physical production mechanism of elephant infrasonic vocalizations. Science. 337(6094):595–599. https://doi.org/10.1126/science.1219712
Hindmarsh MB, Jefferies DJ. 1984. On the motions of the offset impact oscillator. J Phys A Math Gen. 17(9):1791. https://doi.org/10.1088/0305-4470/17/9/015
Karnopp DC, Margolis DL, Rosenberg RC. 2012. System dynamics. Wiley. https://doi.org/10.1002/9781118152812
Kime NM, Ryan MJ, Wilson PS. 2013. A bond graph approach to modeling the anuran vocal production system. J Acoust Soc Am. 133(6):4133–4144. https://doi.org/10.1121/1.4802743
Kime NM, Ryan MJ, Wilson PS. 2019. Modelling the production of complex calls in the túngara frog (*Physalaemus pustulosus*). Bioacoustics. 28(4):345–363. https://doi.org/10.1080/09524622.2018.1458249
Kingsley EP et al. 2018. Identity and novelty in the avian syrinx. Proc Natl Acad Sci USA. 115 (41):10209–10217. https://doi.org/10.1073/pnas.1804586115
Lagorio AD et al. 2020. The arylabialis muscle of the túngara frog (*Engystomops pustulosus*). Anat Rec. 303(7):1966–1976. https://doi.org/10.1002/ar.24267
Lorenz EN. 1963. Deterministic nonperiodic flow. J Atmos Sci. 20(2):130–141. https://doi.org/10.1175/1520-0469(1963)020<0130:dnf>2.0.co;2
Madsen PT, Siebert U, Elemans CP. 2023. Toothed whales use distinct vocal registers for echolocation and communication. Science. 379(6635):928–933. https://doi.org/10.1126/science.adc9570
Martin WF. 1971. Mechanics of sound production in toads of the genus *Bufo*: passive elements. J Exp Zool. 176(3):273–293. https://doi.org/10.1002/jez.1401760304
Negus V, Neil E, Floyd WF. 1957. Lxiv the mechanism of phonation. Ann Otol Rhinol Laryngol. 66 (3):817–829. https://doi.org/10.1177/000348945706600320
Page RA, Bernal XE. 2006. Túngara frogs. Curr Biol. 16(23):R979–R980. https://doi.org/10.1016/j.cub.2006.10.046
Pippard AB. 1978. The driven anharmonic vibrator; subharmonics; stability. Cambridge University Press.
Rand AS, Ryan MJ. 1981. The adaptive significance of a complex vocal repertoire in a neotropical frog. Z Tierpsychol. 57(3–4):209–214. https://doi.org/10.1111/j.1439-0310.1981.tb01923.x
R Core Team. 2025. R: a language and environment for statistical computing (version 4.5.2) [Computer software]. Vienna, Austria: R Foundation for Statistical Computing. https://www.R-project.org/
Ryan MJ. 1980. Female mate choice in a neotropical frog. Science. 209(4455):523–525. https://doi.org/10.1126/science.209.4455.523
Ryan MJ. 1985. The túngara frog: a study in sexual selection and communication. University of Chicago Press. https://doi.org/10.1126/science.231.4743.1317
Ryan MJ, Fox JH, Wilczynski W, Rand AS. 1990. Sexual selection for sensory exploitation in the frog *Physalaemus pustulosus*. Nature. 343(6253):66–67. https://doi.org/10.1038/343066a0
Ryan MJ, Tuttle MD, Rand AS. 1982. Bat predation and sexual advertisement in a neotropical anuran. Am Nat. 119(1):136–139. https://doi.org/10.1086/283899
Tournat V, Gusev VE, Castagnède B. 2004. Subharmonics and noise excitation in transmission of acoustic wave through unconsolidated granular medium. Phys Lett A. 326(5–6):340–348. https://doi.org/10.1016/j.physleta.2004.04.042
Wilczynski W, Rand AS, Ryan MJ. 1995. The processing of spectral cues by the call analysis system of the túngara frog, *Physalaemus pustulosus*. Anim Behav. 49(4):911–929. https://doi.org/10.1006/anbe.1995.0123